Surprising conductive- and dielectric-system dispersion differences and similarities for two Kohlrausch-related relaxation-time distributions

J Ross Macdonald

Department of Physics and Astronomy, University of North Carolina, Chapel Hill, NC 27599-3255, USA

E-mail: macd@email.unc.edu

Abstract

General distributions of relaxation times are discussed and then specialized to two types associated with Kohlrausch stretched-exponential temporal response, the K0 and K1 models. For the important choice of 1/3 for their beta shape parameters, their specific distributions and different temporal responses are first compared. Then the 16 real and imaginary parts of their dielectric- and conductive-system frequency responses are presented in normalized form. Only eight of these are distinct, however, because of pairing of identical dielectric and conductive responses. There are five different peaked imaginary-part pairs, two of which differ only in scale: the important conductive-system $M''(\omega)$ response and the dielectric-system $\varepsilon''(\omega)$ one. Their near equality explains how the widely used but inappropriate original modulus formalism (OMF) of Moynihan and associates, proposed in 1973, could be implicitly derived from pure dielectric considerations and yet fortuitously yield conductive-system response. The crucial effects of the endemic dielectric quantity $\varepsilon_{D\infty}$ on K0- and K1-model responses are illustrated, and they explain why conductive-system shape parameter values derived from data fitting with the OMF model have been misleadingly found to depend on temperature and charge-carrier concentration. Instead, the K1 model fits data for a wide variety of homogenous materials with a value of 1/3 independent of the values of these variables. Finally, different fits of a historic experimental data set are compared to illustrate the present findings.

Important acronyms and names

The addition of a C to a model designation, as in CK0, indicates the presence of a parallel capacitance representing ε_∞ for the K0 model and $\varepsilon_{D\infty}$ for the K1 one. The addition of an S

to a composite model, as in CK1S, indicates the presence of a series constant-phase-element electrode-polarization element in the model.

CMF corrected modulus formalism
CSD conductive-system dispersion
DRT distribution of relaxation times
DSD dielectric-system dispersion
KD Kohlrausch DSD response model; K0 model with shape parameter β_D
K0 Kohlrausch CSD response model or DSD one (K0 DSD); shape parameter β_0
K1 Kohlrausch-derived CSD or DSD response model; shape parameter β_1
OMF original modulus formalism; K1 model with shape parameter β_{1M}
SE stretched exponential; see equation (1)
UN the K1 CSD model with its shape parameter, β_1, fixed at 1/3

1. Introduction

There has been considerable confusion associated with dispersive frequency responses arising from different distributions of relaxation times (DRTs), confusion to which I have contributed my share. Therefore, a purpose of the present work is to try to resolve such past confusion and to explore and compare different response possibilities. To do so, I start with a single seed: the important Kohlrausch stretched-exponential (SE) temporal response,

$$\phi_k(t) = \exp[-(t/\tau_o)^{\beta_k}] \qquad 0 < \beta_k \leqslant 1, \tag{1}$$

with $k = D$ or 0, as discussed below. I then investigate the tree that grows out of this seed, how it exfoliates, and then how its myriad temporal and frequency-domain results may be differentiated. In the frequency domain one deals with immittances, and the results of primary theoretical and experimental interest are those that show dispersed peaked response. Further, it is they that yield the important similarities and differences discussed herein. The choice of equation (1) is relevant both because of its endemic appearance in past experimental and theoretical work and because it leads, with a specific fixed choice of β_k, to frequency response that fits data for a wide variety of materials, temperatures, and charge-carrier concentrations. A list of acronyms is given above.

In the present work, I follow conventional usage of the word 'relaxation' as applied to electrical responses, although it should properly be replaced by 'retardation' [1]. Further, I use 'relaxation' as a blanket term indicating decay from an initial state to a final one when referring to relaxation times and DRTs. In 1994 Phillips suggested that relaxation in complex (disordered) systems is one of the most important unsolved problem in physics today [2], and it is still a source of mystery, inadequate understanding, and opportunity.

More specifically, it is useful to make the distinction between relaxation of Debye type that involves only a single relaxation time, and dispersive relaxation, where either many discrete response times are present or a continuous distribution of response terms is an appropriate description of the situation. Here, as usual, the work is concerned with continuous DRTs, although discrete and continuous DRT responses have been discussed in, for example, [3–5].

Some of the complexity and misunderstanding present in the area of dispersive frequency response arises from the existence of such response involving either dielectric-system dispersion (DSD) or conductive-system dispersion (CSD), commonly represented by either a distribution of dielectric relaxation times or by one of resistivity relaxation times, respectively. In the past, actual CSD data sets, which often show thermally activated response with essentially the same activation energy for the dc resistivity, ρ_0, and for the characteristic relaxation time

Table 1. Comparison of notations for relaxation-time distribution functions. Here, τ_o is the characteristic relaxation time of the response model. DSD or CSD describe the type usually involved, and the integration limits for normalization are listed as $\{a, b\}$.

Some previous and current work; refs.	Tau variables: τ $x \equiv \tau/\tau_o$	Tau variable: $y \equiv \ln(\tau/\tau_o) = \ln(x)$. See equations (2)–(4)
Böttcher and Bordewijk; [6]	$g(\tau) \{0, \infty\}$	$G(\ln \tau) = \tau g(\tau) \{-\infty, \infty\}$ DSD
Moynihan *et al*; [7]	$g(\tau)$ $\{0, \infty\}$	Not identified, but their table 1 presents approximate $\tau g(\tau)$ DSD values. See corrected results in figure 1 of [9]
Lindsay and Patterson; [8]	$\rho(\tau) \{0, \infty\}$	$G(\tau) = \tau \rho(\tau) \{-\infty, \infty\}$ DSD
Macdonald; [9–11]	$G(\tau), G_D(\tau)$ $G_0(x) \equiv \tau_o G_0(\tau)$ $\{0, \infty\}$	$F(y) \equiv \tau G(\tau) \{-\infty, \infty\}$ DSD $G_1(x) = (x/\langle x \rangle_0) G_0(x)$ CSD $\{0, \infty\}$
This work	$g_0(\tau) = g_D(\tau)$ $g_k(\tau) \{0, \infty\}$	$F_0(y) \equiv \tau g_0(\tau) \{-\infty, \infty\}$ CSD, DSD $F_1(y) \equiv x F_0(y)/\langle x \rangle_{01}, \{-\infty, \infty\}$ CSD

of the response, τ_o, have often been characterized as involving dielectric response, perhaps because the data were shown and analysed at the dielectric immittance level. As we shall see, however, there are significant differences between CSD data presented at the complex dielectric level and DSD data at that level. Dispersive CSD data sets involve mobile charged entities (monopoles), while dispersive DSD ones involve dipoles and possibly higher multipoles.

For easy comparison, all synthetic responses are presented in normalized form. Section 2 first deals with DRTs in general, especially their three levels, and then compares the two most important ones graphically for specific Kohlrausch DRT response choices. Next, in section 3, the accurate temporal responses following from these DRTs are briefly discussed. Then in section 4, all normalized DSD and CSD immittance frequency responses for the important choice $\beta = 1/3$ are illustrated and compared, with emphasis on the five possible imaginary-part peaked responses. Section 5 compares the still widely used original modulus formalism (OMF) frequency response with its corrected version (the CMF) and shows how misconceptions in the derivation of the OMF nevertheless led to important but misinterpreted results. Section 6 then shows how normalized CSD responses are modified by the presence of the frequency-independent pure dielectric constant quantity $\varepsilon_{D\infty}$, while section 7 compares fitting of the frequency-response data of an ionic glass with OMF and CMF conductive-system-dispersion models, with and without taking account of electrode polarization effects.

2. Distributions of relaxation times

Since a long, general review of DRTs and their responses is available [3], it is sufficient here to begin by comparing different general DRT notations and relations and only then to consider three specific DRT types associated with the SE response of equation (1). Table 1 includes a partial list of DRT notations used by different authors. Although all these DRTs may be used to generate either DSD or CSD response, these terms are included in the table to indicate either the provenance of the work cited and/or the actual type involved.

In table 1, k-subscript values of D, 0, and 1 are included, with the $k = 1$ choice involving equation (1) only indirectly, as discussed below. Because there is no difference in form between the $k = D$ and 0 DRTs, the $k = 0$ designations apply to both here but their distinction is needed for CSD and DSD situations. Those designations without a subscript, such as $F(y)$,

implicitly involve either $k = D$ or 0 subscripts. Note that the DRTs in column two that involve an argument of τ have the dimension of that of τ^{-1}, while those in column three are dimensionless. The normalized τ variable in column three is $x \equiv \tau/\tau_o \equiv \exp(y)$.

So far we are still dealing with general DRTs, and relevant equations connecting important quantities are

$$\phi_k(t) = \int_0^\infty \exp(-t/\tau)g_k(\tau)\,\mathrm{d}\tau = \int_{-\infty}^\infty \exp[-(t/\tau_o)\exp(-y)]F_k(y)\,\mathrm{d}y \quad (2)$$

and

$$I_k(\omega) = I_k' \pm \mathrm{i}I_k'' \equiv \frac{U_k(\omega) - U_k(\infty)}{U_k(0) - U_k(\infty)} = \int_0^\infty \frac{G_k(x)}{[1 + \mathrm{i}\omega\tau_o x]}\,\mathrm{d}x = \int_{-\infty}^\infty \frac{F_k(y)}{[1 + \mathrm{i}\omega\tau_o \exp(y)]}\,\mathrm{d}y \tag{3}$$

for temporal and frequency responses. Here $I_k(\omega)$ is the normalized frequency response and $U_k(\omega)$ may represent any of the four immittances, $\rho(\omega)$, $M(\omega)$, $\sigma(\omega)$, or $\varepsilon(\omega)$: the complex resistivity, the complex modulus, the complex conductivity, and the complex dielectric constant, respectively, expressed in specific form. The $k = D$ choice (with $\pm \to -$), where $U_D(\omega) = \varepsilon_D(\omega)$, selects the DSD situation, while the $k = 0$ or 1 (with $\pm \to +$) ones are appropriate for two types of $U_k(\omega) = \rho_k(\omega)$ CSD response.

So far so good when the form of a DRT is known, but here we want to start with a known temporal response, such as the stretched exponential of equation (1), and find expressions for the DRTs associated with it, a difficult problem that is discussed in detail in [12]. Although an expression for $g_k(\tau)$ may be obtained [8, 12] by taking a Fourier–Laplace transform of the $\phi_k(t)$ of equation (2), when the specific SE form is used, closed-form analytic expressions for $g_k(\tau)$ with $k = D$ or 0 are only available for $\beta_k = 1/3, 1/2, 2/3,$ and 1.

Therefore, the formulae for the first two of these β_k values and special series ones for $0 < \beta_k < 1$ are used in the LEVM complex-nonlinear-least-squares fitting and inversion computer program [13] to obtain values of $F_k(y) = \tau g_k(\tau)$ for $k = D$ or 0, and for

$$F_1(y) \equiv x F_D(y)/\langle x \rangle_{D1} \equiv x F_0(y)/\langle x \rangle_{01}. \tag{4}$$

At least five-figure accuracy of these DRTs is available for the range $0.2 \leqslant \beta_k \leqslant 0.8$ and it is somewhat less outside this range. Although $F_1(y)$ may be calculated from either the $k = D$ DSD or the equivalent $k = 0$ CSD DRT, it turns out to be of primary importance for experimental CSD situations. Here, $\langle x \rangle_{k1}$ is the average over the appropriate normalized DRT for $k = D$ or 0, given by

$$\langle x \rangle_{k1} = \beta_k^{-1}\Gamma(\beta_k^{-1}), \tag{5}$$

where Γ is the Euler gamma function [8]. It follows that $\langle x \rangle_{01}$ equals 2 or 6 for $\beta_k = 1/2$ or $1/3$, respectively. The $k1$ subscript indicates that the average is over the $F_k(y)$ DRT involving the β_1 value. When the form of $\phi_k(t)$ is known, one can calculate $\langle \tau \rangle_k \equiv \tau_o \langle x \rangle_k$ from $\langle \tau \rangle_k = \int_0^\infty \phi_k(t)\,\mathrm{d}t$ [7, 8].

Figure 1 shows some Kohlrausch distributions for several values of $(\mathrm{K}k, \beta_k)$, where $\mathrm{K}k$ denotes ones derived from SE Kohlrausch temporal response, as discussed above. We shall use KD, K0, and K1 to designate these DRTs and, as well, the temporal and frequency response models that follow from them when they are used in equations (2) and (3). The unnormalized $(k, \beta_0) = (1, 1/3)$ dashed F_1 curve was formed from the $(0, 1/3)$ F_0 one by multiplying the latter by $x \equiv \tau/\tau_o$, where τ_o is fixed at a normalization value of 1 s for all synthetic data results in the present work. Thus, the $(0, 1/3)$ and unnormalized $(1, 1/3)$ values are equal at the $x = 1$ point. The unnormalized curve was then normalized by dividing by $\langle x \rangle_{01} = 6$ to give the proper $F_1(y)$ distribution.
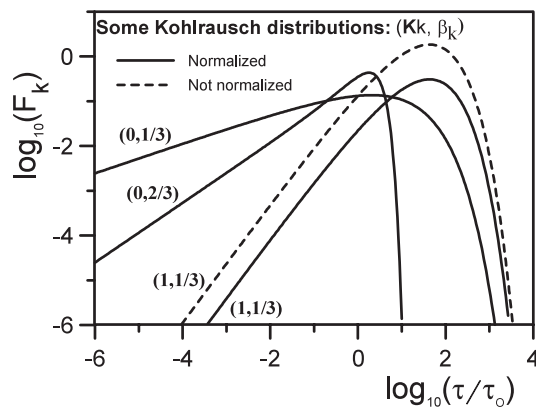
Figure 1. Comparison of several Kohlrausch-derived distributions of relaxation times for Kk models (with $k = 0$ or 1) for β_0 equal to 1/3 and 2/3 and $\beta_1 = 1/3$. Here and hereafter $\tau_o = 1$ s.

In addition to the $\beta_k = 1/3$ results shown in the figure, a $(0, 2/3)$ DRT curve is also included because it turns out that the corresponding CSD K0 frequency-response curve with $\beta_0 = 2/3$ and the CSD K1 one with $\beta_1 = 1/3$ both lead to a high-frequency limiting log–log slope of $\sigma'(\omega)$ of 2/3 [14, 15], although their DRTs are evidently quite different. Finally, the peak value of the $(0, 1/3)$ and $(1, 1/3)$ DRT curves are about 0.137 and 0.308, respectively, while those for $(0, 1/2)$ and $(1, 1/2)$ are about 0.242 (as in figures 1 and 3 of [9]) and 0.462, respectively.

3. K0 and K1 temporal responses

Since $\phi(t)$ response curves have been discussed previously for SE models with various values of β as well as for some other models [14, 16, 17], only the temporal responses following from the DRTs of figure 1, using equation (2), are considered here and are shown in figure 2. The $(0, 1/3)$ and $(0, 2/3)$ curves are necessarily of exact SE form. Even though the $(1, 1/3)$ curve appears quite similar to the $(0, 2/3)$ one except for displacement in time, it is appreciably different. Not only do the two responses differ in their shapes in the $0.7 < \phi < 1$ region but log–log plots show that they approach zero appreciably differently. In fact, when the $(1, 1/3)$ data were fitted with a $(0, \beta_0)$ SE model, the relative standard deviation of the fit, S_F, turned out to be about 0.04 and the β_0 estimate was close to 0.53.

Specific deviations of the $(1, 1/3)$ data from SE form are discussed in [17]. Finally, note that ϕ_D behaviour (formally the same as that of the ϕ_0 curves shown) is closely related for DSD situations to the transient current response resulting on application of a step function potential to the material, or to discharge from a fully charged condition. The normalized transient current for either situation is directly related to $-d\phi_D/dt$ [8]. For CSD situations, however, the ϕ_k curves of figure 2 represent charge-carrier correlation functions [14, 17].

4. All K0- and K1-model frequency responses

These responses are calculated using in equation (3) the F_0 and F_1 DRTs discussed in section 2. We begin with the calculation of $I_k(\omega)$ results, for $k = 0$ and 1, separately for DSD and CSD situations, all with $\beta_k = 1/3$. Thus all such results are normalized and represent only basic K0- and K1-model responses for these situations. Where needed, let C and D subscripts denote

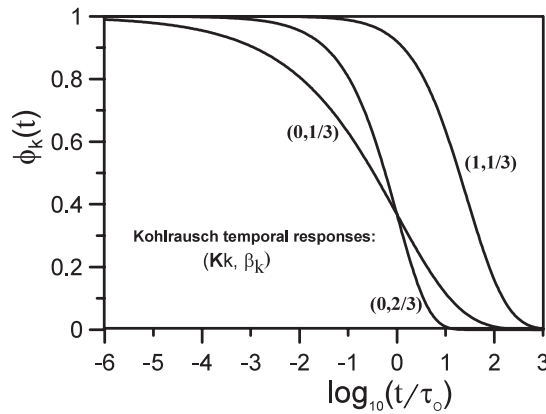**Figure 2.** Comparison of three ϕ_k temporal response functions associated with the normalized DRTs of figure 1. The $(1, 1/3)$ one follows from the normalized $(1, 1/3)$ DRT of figure 1, not from the un-normalized one.

CSD and DSD situations and response quantities. It is worth emphasizing, however, that since we shall often use the K0 designation to include both the KD model (which involves a DSD relaxation-time distribution) and a CSD situation associated with a resistivity DRT, a K0 model will usually be qualified with either DSD or CSD as necessary.

The actual calculations, using LEVM and $k = 0$ and 1, involved the DSD normalization choices $\varepsilon_k(0) = \varepsilon'_D(0) \equiv \varepsilon_{D0} = 1$, $\varepsilon_k(\infty) = \varepsilon'_D(\infty) \equiv \varepsilon_{D\infty} = 0$, and $\tau_o = 1$ s, and the CSD ones $\rho_k(0) = \rho_{C0} = \rho_0 = 1$ Ω cm, $\rho_k(\infty) = \rho_\infty = 0$, and $\tau_o = 1$ s. These choices lead, for example, to the normalized CSD response $I_1(\omega) = U_1(\omega)/U_1(0) = \rho_1(\omega)/\rho_0 \equiv \rho_C$, and to the normalized DSD response $I_0(\omega) = U_0(\omega)/U_0(0) = \varepsilon_0(\omega)/\varepsilon_{D0} \equiv \varepsilon_D$. There are separate normalized response quantities, both denoted by ρ_C and ε_D, for the K0 and K1 models.

The general relations between the four different immittances are $M = i\omega\varepsilon_V\rho$, $\sigma = i\omega\varepsilon_V\varepsilon$, $\varepsilon = 1/M$, and $\rho = 1/\sigma$, where ε_V is the permittivity of vacuum. When applying these relations to calculate the three remaining normalized responses from either the normalized quantity ρ_C or ε_D for either CSD or DSD situations, respectively, it is appropriate to set ε_V equal to 1 s rad^{-1} in order for all the resulting immittances, such as ε_C or ρ_D, to be normalized as well.

The second column of table 2 shows all the various normalized immittance notations for the K0 and K1 models. Note that because each of the listed pairs is calculated from the same DRT, such responses as ρ_C and ε_D for a given Kk model are exactly the same but apply at different immittance levels. The bold-faced numbers in column 2 of the table denote those responses whose imaginary parts are of peaked character, ones of particular interest. For the rows designated by the numbers **4** and **5**, the peaked CSD imaginary-part response is that of ε_C after subtraction of the effects of ρ_0; thus it is denoted ε''_{CS}. In table 2, ν_p is the frequency at the peak of any peaked imaginary-part response and $\tau_p \equiv 1/(2\pi\nu_p)$ is the corresponding value of τ at the peak. In addition to the high-frequency limiting slopes of quantities listed in column 2, the table also includes the value of the width parameter W for peak-response curves. For Debye relaxation response, $W \cong 1.144$, the minimum value, that when dispersion is absent.

As table 2 shows, there are only four different immittance response pairs or duals, and results are shown for each of them for the K0 and the K1 models. The real and imaginary parts of all these responses are shown in figures 3 and 4 and include the number identifications of the second column of table 2 where appropriate. Note especially in the bottom panel of figure 4 that the K0 and K1 imaginary parts of ε_C and $-\rho_D$ approach equality in the low-frequency
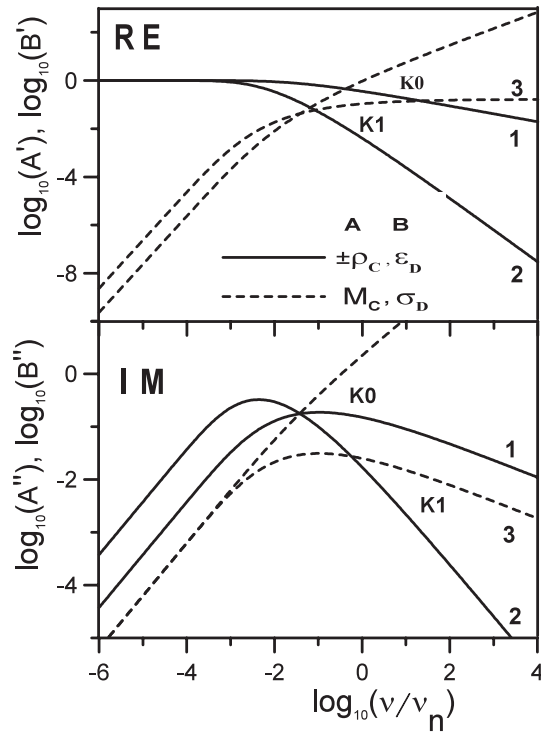
Figure 3. Comparison of real- and imaginary-part normalized frequency responses for K0 and K1 models representing conductive systems (subscript C) and dielectric ones (subscript D) at different immittance levels. See table 2 for further letter and number information, including high-frequency slope values. As usual, $-\rho''$ values are plotted along with ρ' values here and in figures 4 and 5. Here and hereafter $\nu_n = 1$ Hz.

Table 2. Normalized dispersion results for $\beta_k = 1/3$. Here IL denotes the immittance level, and C and D subscripts stand for conductive-system dispersion and dielectric-system dispersion types, respectively. The HF slope is the high-frequency-limiting log–log slope of a response curve, and W is defined as $\log(\omega_{+1/2}/\omega_{-1/2})$, where the $\omega_{\pm 1/2}$ values are those at half-height of a peaked dispersion curve. Quantities in parentheses are associated with ε''_{CS}. The identifying numbers **1–5** in column 2 are used in figures 3–5. ν_p is the peak frequency and $\nu_n \equiv 1$ Hz.

Model	No., (IL)$_{\text{Type}}$	Peak height	ν_p/ν_n	τ_p/τ_o	HF real-part slope	HF imag.-part slope	Width W
K0	**1** ρ_C, ε_D	0.1869	0.106 4	**1.495**	$-1/3$	$-1/3$	**3.251**
K1	**2** ρ_C, ε_D	0.3254	0.004 403	36.15	-1	$-4/3$	1.894
K0	M_C, σ_D	—	—	—	$2/3$	$2/3$	—
K1	**3** M_C, σ_D	0.0312	0.106 4	**1.495**	0	$-1/3$	**3.251**
K0	**4** ε_C, ρ_D	(1.732)	(0.004 878)	(32.63)	$-2/3$	$-2/3$	(2.108)
K1	**5** ε_C, ρ_D	(14.41)	(0.001 787)	(89.06)	0	$-1/3$	(2.183)
K0	σ_C, M_D	—	—	—	$1/3$	$1/3$	—
K1	σ_C, M_D	—	—	—	1	$2/3$	—

region and that even after subtraction of ρ_0 effects, they both approach their unsubtracted values in the high-frequency region but are appreciably different at lower frequencies.

The observant reader may be surprised that figure 4 shows non-zero values of $\rho_{Dk0} \equiv \rho'_{Dk}(0)$ for both of the K0 and K1 curves, unexpected for a pure dielectric situation that
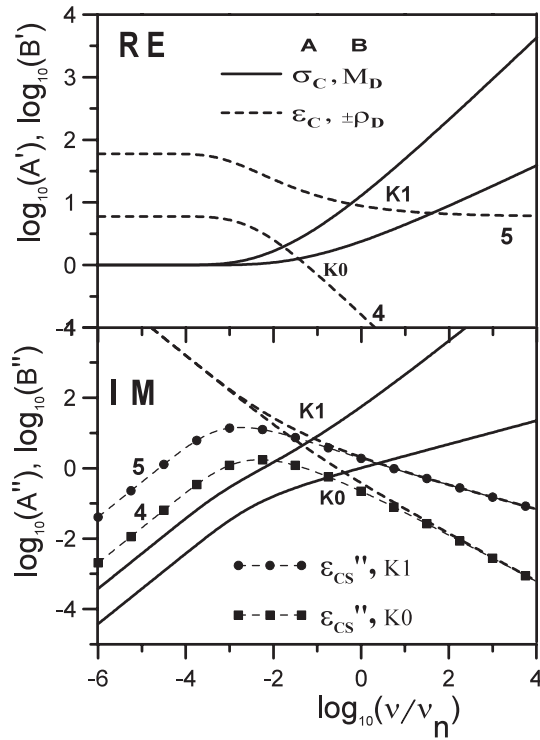
Figure 4. Comparison of further real- and imaginary-part normalized frequency responses for K0 and K1 models representing conductive systems and dielectric ones at different immittance levels. In forming the ε_{CS}'' responses, the effect of ρ_0 has been subtracted.

involves no mobile-charge effects. It turns out for the present normalized parameters with the $\beta = 1/3$ choice that for the K0 model $\rho_{D00} = \varepsilon_{C00} = \varepsilon_{C1\infty} = 6$, and for the K1 $\rho_{D10} = \varepsilon_{C10} = \Gamma(6)/\Gamma(3) = 60$ [8, 10, 14]. An expression for $\varepsilon_{C1\infty}$ is presented in the following section. These results follow because in the general CSD case, where ρ_∞ is not necessarily 0 and $\Delta\rho \equiv \rho_0 - \rho_\infty$, one can first write, for $k = 0$ or 1,

$$\varepsilon_{Ck0} = [(\Delta\rho)_k/\{\varepsilon_V(\rho_{Ck0})^2\}]\langle\tau\rangle_k, \tag{6}$$

where, as usual, we use $\rho_0 = 1/\sigma_0$ to represent ρ_{Ck0} for either value of k. The dual of this equation, written for DSD conditions with $k = D$, is just [18]

$$\rho_{D0} = [(\Delta\varepsilon)_D/\{\varepsilon_V(\varepsilon_{D0})^2\}]\langle\tau\rangle_D, \tag{7}$$

where $\varepsilon_{D0} \equiv \varepsilon_{D00}$ and $(\Delta\varepsilon)_D \equiv \Delta\varepsilon_D \equiv \varepsilon_{D0} - \varepsilon_{D\infty}$. Although a pure dielectric system thus leads to a non-zero ρ_{D0}, the results in figure 3 indicate that σ_{D0} is zero, in accordance with physical reality.

Figure 5 shows complex-plane plot results for the three unsubtracted pairs that involve peaked imaginary-part response and linear plots for all five peaked imaginary-part responses, all normalized to peak heights of unity. As the figure shows, although the imaginary-part responses for the pairs identified as **1** and **3** in table 2 are identical when further normalized in this fashion, their complex-plane responses are mirror images and the arrowheads show the direction of increasing frequency.
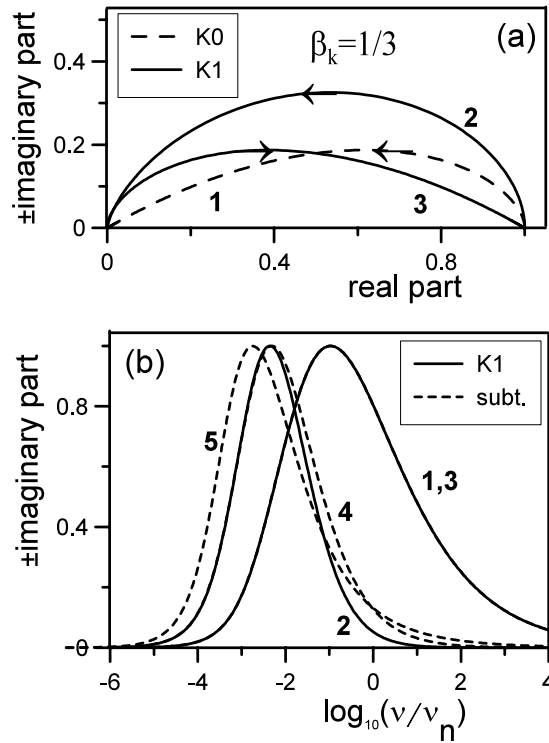
Figure 5. (a) Normalized complex-plane responses for $\beta_k = 1/3$ for the situations designated by the numbers **1**–**3** in table 2. The arrows show the direction of increasing frequency. (b) Imaginary-part responses, all normalized to a peak height of 1, for the situations designated by the numbers **1**–**5** in table 2.

5. CSD and DSD surprises

Recent work [14, 15, 17, 19] has demonstrated that the CSD K1 model with $\beta_1 = 1/3$ fits a wide variety of experimental frequency-response data for homogeneous glasses and single crystals over appreciable ranges of temperature and concentration. Because this conclusion is supported by both theory and experiment, the resulting model has therefore been denoted by UN or U to emphasize its quasi-universality. Although such fits generally require that the effects of the frequency-independent dipolar dielectric constant, $\varepsilon_{D\infty}$, and of electrode polarization be separately included in a composite model, as discussed in sections 6 and 7, here we continue to deal just with the basic K0 and K1 responses described in section 4.

A ground-breaking macroscopic derivation and application of the K1 model for CSD frequency-response situations appeared in 1973 [7], and its teachings have been used in a great many other publications up to the present. Because of this widespread use, even after a crucial defect in it was identified ten years ago, its further consideration seems justified. It made use of the present equations (1) and (2) and also of

$$I_k(\omega) = \int_0^\infty \exp(-i\omega t)\left(-\frac{d\phi_k(t)}{dt}\right) dt, \tag{8}$$

for $k = D$ or 0, a one-sided Fourier transform that connects $I_k(\omega)$ and $\phi_k(t)$. Since the K0 model for fitting CSD data was not introduced until 1997 [10], it is clear that for the

1973 derivation k should be set to D in the above equation and also in equations (1) and (2), or equivalently, to 0 with the proviso that a DSD situation is involved. In fact, the $I_D(\omega)$ introduced in [7], and denoted $N^*(\omega)$ there, may be directly identified with the normalized K0 DSD $\varepsilon_D(\omega)$ quantity listed as No. **1** in table 2 and in figure 3, although Moynihan *et al* [7] show a plot of it for $\beta_0 = 1/2$ rather than 1/3.

These results lead to a surprising and hitherto unrecognized anomaly: how does a K0 DSD analysis lead to a K1 CSD response model? The answer is somewhat subtle and complicated, possibly explaining why the matter has escaped attention for 32 years. In brief, the reference [7] derivation works because of a remarkable coincidence: namely, that except for a scaling difference associated with $\langle x \rangle$, table 2 and figure 3 show that the imaginary parts of the K0 $\varepsilon_D(\omega)$ response, identified by the bold-faced number **1**, and that of the K1 $M_C(\omega)$, identified by the number **3**, are identical. For the present $\beta_1 = 1/3$ choice, the peak value of the K0 responses marked **1** in table 2 are just six times larger than those for the K1 responses marked **3**.

Therefore, if one deals only with CSD K1-model $M_C''(\omega)$ response in fitting data, a DSD KD = K0 $\varepsilon_D''(\omega)$ response model may be used to analyse such CSD response! In fact, the Moynihan *et al* approach [7] has been referred to as the modulus formalism model and has been widely used to estimate β_1 by the width parameter, W, of experimental $M''(\omega)$ peaked response curves. Since W, as defined in the caption of table 2, is independent of the actual peak height of such a curve, the difference in scaling mentioned above and associated with the use of a K0 DSD rather than a K1 CSD one, does not matter. The results of the reference [7] model have been called the original modulus formalism (OMF) to distinguish it from the corrected version described below.

So much for the mechanics of the OMF derivation, but what about its physics? The reference [7] approach, based in part on earlier mechanical relaxation equations and on the decay of an electric field at constant displacement, was used to analyse modulus-level CSD response that involved $\rho_\infty = 0$. It may be expressed in the present notation as

$$M_{C1}(\omega) = M_{C1}'(\omega) + iM_{C1}''(\omega) = i\omega\varepsilon_V\rho_0 I_1(\omega) \equiv [1 - I_{01}(\omega)]/\varepsilon_Z, \qquad (9)$$

where the important effective-dielectric-constant quantity $\varepsilon_Z \equiv 1/M_{C1}'(\infty)$ was defined as $\varepsilon_{D\infty}$ or, equivalently at that time, as ε_∞. Only when the $I_{01}(\omega)$ term in equation (9) is derived from SE response, through the use of equations (2) and (8), should the general equation (9) be then identified as a K1 response model, however. It is also worth mentioning that a normalized expression formally equivalent to the Moynihan *et al* derivation of their version of equation (9) (equation (3) of [7]) appeared ten years earlier [1, equation (A2)]. It applies to either electrical or mechanical relaxation situations and involves an $I_0(\omega)$ term consistent with the present equation (3). Nevertheless, Moynihan *et al* [7] deserve much credit for first applying their results to charged-carrier dispersion situations.

As pointed out since 1995 (e.g., [9, 19, 20]), the OMF identification of ε_Z is incorrect since it introduces a dipolar-related dielectric constant into a purely mobile-charge CSD response equation, and in addition, it leads to inconsistent response at different immittance levels [20]. The remaining problem is that in the OMF $I_{01}(\omega)$ is the DSD KD = K0 response model involving a $\beta_D = \beta_0$ value equal to the CSD K1 β_1 value. See also the later DSD treatment of [8]. But clearly, consistency should require that a mobile-charge-carrier CSD expression such as equation (9) should not involve a pure dielectric dipolar response function such as $I_0(\omega) = I_D(\omega)$, and so the $I_{01}(\omega)$ of equation (9) should be interpreted as involving only CSD mobile-charge response.

In fact, a proper derivation of K1-model response, based on the $F_1(y)$ DRT of table 1 [9, 10, 21] yields the M_C and σ_D responses designated by **3** in table 2, and also leads

to just the above equation (9) result, but with a different explicit expression for ε_Z in the CSD situation, as well as an $I_{01}(\omega)$ result associated only with mobile charge. Because the OMF was incorrectly associated with ε_D, itself directly derived from DSD SE temporal response, it is tempting but incorrect to associate the $k = 1$ K1-model $I_1(\omega)$ directly with SE response by using equations (2) and (8). In fact, accurate calculations of $\phi_1(t)$ response using equation (2) with $\beta_1 = 1/3$ lead to appreciably different behaviour which only reduces to SE response in the long-time limit. In actual calculations of K1 frequency response, it is more appropriate to use its DRT in equation (3) than to use equation (9) because of inaccuracies in the calculation of $1 - I_{01}(\omega)$ at low frequencies.

The macroscopic equation (9) derivation of $M_{C1}(\omega)$ is consistent with the 1973 pioneering continuous-time-random-walk microscopic theoretical analysis of Scher and Lax [22], which, with a minor addition [21] and the specific choice of SE $\phi(t)$ temporal response, also leads to the CSD K1 model of equation (9). The latter, especially with the theoretically predicted value of $\beta_1 = 1/3$ [14, 17], the UN model, is the only available one justified by both macroscopic and microscopic approaches that yields excellent fits of both the real and imaginary parts of experimental frequency-response data for homogeneous materials.

When the OMF analysis is corrected as above, resulting in the corrected modulus formalism (CMF) CSD K1 model, one finds that the appropriate expression for ε_Z is

$$\varepsilon'_{C1}(\infty) \equiv \varepsilon_{C1\infty} = (\sigma_0/\varepsilon_V)/\langle \tau^{-1} \rangle_1 \equiv \varepsilon_{Ma}/\langle x^{-1} \rangle_1 = \varepsilon_{Ma}\langle x \rangle_{01} = [\gamma N(qd)^2/(6k_B\varepsilon_V)]/T.$$
(10)

The high-frequency-limiting effective dielectric constant, $\varepsilon_{C1\infty}$, associated entirely with mobile-charge effects, is likely to arise from the short-range vibrational and librational motion of caged ions. Here $\varepsilon_{Ma} \equiv \sigma_0\tau_o/\varepsilon_V$, involving the mobile-charge σ_0 and τ_o parameters. The quantity N is the maximum mobile-charge number density; γ is the fraction of charge carriers of charge q that are mobile; d is the rms single-hop distance for a hopping entity, and k_B is the Boltzmann constant.

6. Effects of $\varepsilon_{D\infty}$

Since the effects of $\varepsilon_{D\infty}$ on frequency response were purposely omitted from the above basic-response analyses, it is important to discuss these effects since they may be of great importance in the analysis of actual experimental data. The endemic high-frequency-limiting quantity $\varepsilon_{D\infty}$ is frequency independent in the range of usual immittance spectroscopy measurements. For the un-normalized DSD situation, one writes $\varepsilon_D(\omega) = \varepsilon_{D\infty} + \Delta\varepsilon_D I_D(\omega)$ with $\varepsilon_{D\infty}$ and $\Delta\varepsilon_D$ taken as separate fitting parameters. It reduces to the normalized Kohlrausch K0 = KD $\varepsilon_D(\omega)$ response discussed above when $\varepsilon_{D\infty}$ is set to zero and $\Delta\varepsilon_D$ to unity.

For the important CSD situation in the usual absence of DSD, the effects of $\varepsilon_{D\infty}$ are generally more complicated because mobile-charge dispersion leads to a new high-frequency-limiting capacitative contribution, the $\varepsilon_{C1\infty} \equiv \varepsilon'_C(\infty)$ quantity of equation (10), when the data are best represented by the $k = 1$ $F_1(y)$ DRT. The total high-frequency-limiting dielectric constant is then $\varepsilon_\infty = \varepsilon_{C1\infty} + \varepsilon_{D\infty}$ [19, 21]. For the CMF UN model, $\varepsilon_{C1\infty}$ is just $6\varepsilon_{Ma}$, and for the normalization used above, $\varepsilon_{Ma} = 1$.

Data fitting with a composite CSD model involving a free dielectric-constant parameter, ε_x, in parallel with the response of a K1 or UN model leads to an estimate of $\varepsilon_x = \varepsilon_{D\infty}$ and an estimate of $\varepsilon_{C1\infty}$ then follows from those of ρ_0 and τ_o. Since $\varepsilon'_C(\infty) = 0$ for the $k = 0$ K0 model, the presence of a free ε_x parameter in a composite K0 fitting model, the CK0, must necessarily lead to an estimate of ε_∞. If the data are most appropriately fitted by a $k = 1$
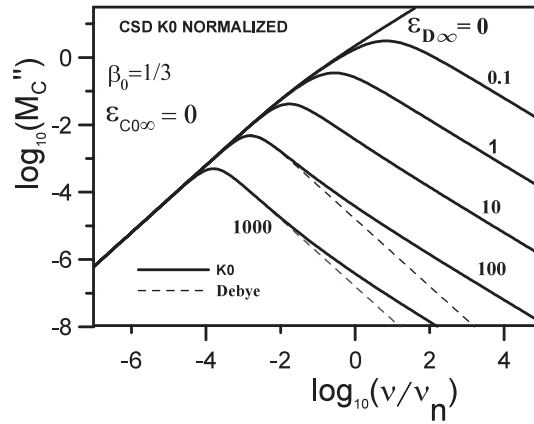
Figure 6. Demonstration of the effect of non-zero $\varepsilon_{D\infty}$ values on normalized M_C'' response for the CK0 model, showing the approach to full Debye response as $\varepsilon_{D\infty}$ increases.

model, however, then the K0 ε_∞ estimate will be that of $\varepsilon_\infty = \varepsilon_{C1\infty} + \varepsilon_{D\infty}$. Otherwise, it follows that the ε_∞ estimate is that of $\varepsilon_{D\infty}$ alone.

The OMF approach [7] uses the CSD K1 fitting model but does not recognize the need for a separate ε_x fitting parameter and the existence of $\varepsilon_{C1\infty}$. Therefore, the OMF ε_Z of equation (10) is forced during fitting to be an estimate of ε_∞, not just $\varepsilon_{C1\infty}$, and it will thus improperly involve the DSD quantity $\varepsilon_{D\infty}$. In consequence, when the expression for the $\langle x \rangle_{01}$ quantity of equation (5) is used in equation (10), an incorrect estimate of β_1 will be obtained. Therefore, the experimentally inconsistent and theoretically inappropriate OMF approach should never be used for fitting and for the estimation of β_1.

Figure 6 shows the results of including $\varepsilon_{D\infty}$ in a composite CSD model, the CK0, one where the K0-model parameters are all normalized as in figures 3 and 4. Since M_C'' response is commonly used and plotted in both the OMF and CMF approaches, it is of most interest to show results at this immittance level, both for K0 and K1 models. As figures 3 and 6 indicate, there is no peaked response present for the K0 model alone because $\varepsilon_\infty = 0$, and such response only appears for non-zero $\varepsilon_{D\infty}$. We see that as $\varepsilon_{D\infty}$ increases, more and more of the response on the high-frequency side of the peak becomes of Debye character and thus more of the original high-frequency curve with a slope of $-2/3$ is replaced by response with a slope of -1. For data of this kind, estimation of β ($=\beta_1$) by the OMF peak-width approach would show this quantity increasing from the present actual β_0 value of $1/3$ for very small $\varepsilon_{D\infty}$ towards a value of unity for large $\varepsilon_{D\infty}$.

The somewhat similar K1-model results of figure 7 are of more interest because of the finding that most CSD data are best fitted with a composite K1 or UN model, the CK1 or CUN, as discussed above. Here $r_{DC} \equiv \varepsilon_{D\infty}/\varepsilon_{C1\infty}$ is the most important response quantity. As it increases from zero, once again any OMF β_1 estimate, which we will denote by β_{1M} to recognize this Moynihan approach, will increase from its appropriate value of $1/3$ when r_{DC} is small towards unity as r_{DC} increases. The complex-plane plots of figure 8(a) show such a progression very clearly.

As discussed earlier [14], as r_{DC} increases the basic UN part of the response becomes a smaller and smaller relative part of the total response, one that becomes dominated by simple Debye response involving ρ_0, $\varepsilon_{D\infty}$, and their relaxation time, $\tau_M \equiv \rho_0\varepsilon_{D\infty}$. It is usually found that $\varepsilon_{D\infty}$ is nearly constant or increases slowly with increasing temperature while equation (10)
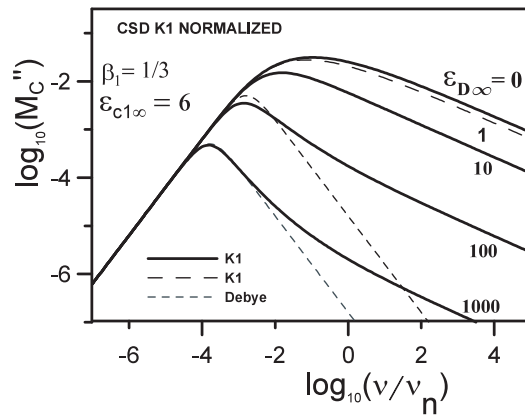
Figure 7. Demonstration of the effect of a non-zero $r_{DC} \equiv \varepsilon_{D\infty}/\varepsilon_{C1\infty}$ ratio on normalized M_C'' response for the CK1 = CUN model, showing the slow approach to overall Debye response as the ratio increases.
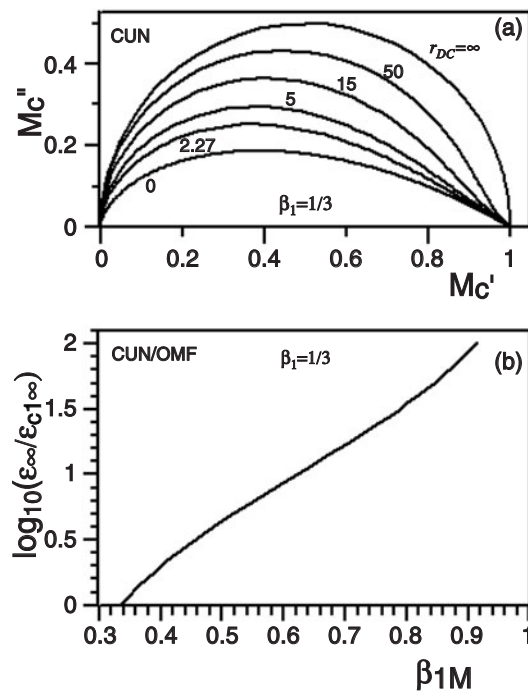

Figure 8. (a) Exact complex-plane M-level normalized response curves using the CUN model for various values of $r_{DC} \equiv \varepsilon_{D\infty}/\varepsilon_{C1\infty}$. The top curve is that for pure dielectric Debye response, appropriate when $\varepsilon_{C1\infty} = 0$, and the bottom one applies for the $\varepsilon_{D\infty} = 0$, a pure conductive-system K1 situation. (b) The line connects β_{1M} values, obtained from original-modulus-formalism (OMF) fitting of exact CUN-model data with the CMF ratio $\varepsilon_\infty/\varepsilon_{C1\infty} = 1 + r_{DC}$. Its equation is $\log_{10}(\varepsilon_\infty/\varepsilon_{C1\infty}) = \sum_{k=0}^{3} a_k(\beta_{1M})^k$, where $a_0 = -2.7689$; $a_1 = 12.652$; $a_2 = -15.844$; and $a_3 = 8.4510$.

indicates that for full dissociation, where N is temperature independent, $\varepsilon_{C1\infty}$ is proportional to $1/T$. Thus, one expects that r_{DC} should usually increase as T increases [19]. Further, we

expect N to be proportional to the relative ionic concentration, again leading to decreasing $\varepsilon_{C1\infty}$ and to increasing r_{DC} as the concentration diminishes [14, 19]. Thus, in both cases, one expects that β_{1M} will increase towards unity, as observed [16, 19, 23].

Because the OMF is properly inapplicable, the above dependences of β_{1M} on temperature and charge-carrier concentration should not be significant, but because hundreds of OMF fits and β_{1M} estimates have been published since 1973, it is still of interest to show their connection with predictions of the widely applicable CUN fitting model. The line of figure 8(b) may be used when a value of β_{1M} is available to obtain a rough estimate of the CUN ratio $\varepsilon_\infty/\varepsilon_{C1\infty} = 1+r_{DC}$, and a more accurate estimate may be obtained using the polynomial-fit equation listed in the figure caption. For situations where an original data set is unavailable for a CUN fit but where OMF-fit estimates of both β_{1M} and $\varepsilon_{\infty M}$ are known, using $\varepsilon_{\infty M}$ as an approximation for ε_∞ allows one to obtain estimates of the associated CUN $\varepsilon_{C1\infty}$ and $\varepsilon_{D\infty}$ values from the present graphical results without further fitting. An example is discussed in the next section.

7. A data-fitting example

In order to illustrate some important features of OMF and CMF fits of CSD data, it is particularly appropriate to show and discuss fitting results for the $Li_2O \cdot Al_2O_3 \cdot 2SiO_2$ (LAS) data set, first analysed in 1973 by Moynihan and associates in [7]. These authors did not show a log–log plot of M' and only plotted results for $\nu \geqslant 1$ Hz. Thus, the curvature of the M' response apparent at the lowest frequencies in figure 9(a) did not appear in their results. Such curvature indicates the presence of electrode polarization effects [15], ones not accounted for in [7]. As the figure shows, a complex-nonlinear-least-squares CUNS-model fit using the LEVM program led to excellent agreement with both the real and imaginary parts of the modulus-level data over the full data range. The composite CUNS fitting model included a series constant-phase element to model such effects, and they have been shown to frequently influence the high-frequency region of the data as well as the low-frequency one [15].

The curves identified as K1-U in figure 9(a) are the result of an OMF fit without correction for electrode effects. In order to obtain results similar to those shown in figure 2 of [7], this fit was carried out using unity weighting, one that emphasizes the large over the small parts of the data. Note its failure to match the data at its high-frequency end, a defect also apparent in figure 2 of [7]. Such discrepancies have been widely observed in OMF fitting and were characterized as 'endemic' in [7]. Over the years many unconvincing explanations for such behaviour have been proposed, but, as comparison of the two fits shown in figure 9(a) indicates, electrode polarization is the proper explanation.

The Moynihan *et al* OMF fit of the LAS data led to the estimated parameter values $\beta_{1M} = 0.47$, $\tau_o = 4.0 \times 10^{-4}$ s, $\varepsilon_\infty = 9.09$, and $\varepsilon_0 = 25$–35. For comparison, the parameter estimates obtained from the complex K1-U fit of figure 9(a) were $\beta_1 = 0.447$, $\tau_o = 3.87 \times 10^{-4}$ s, $\varepsilon_\infty = 8.99$, $\varepsilon_0 = 35.6$, and $\rho_0 = 1.22 \times 10^9$ Ω cm. When this fit was repeated including electrode-polarization parameters and proportional weighting, more appropriate parameter estimates were $\beta_{1M} = 0.468$, $\tau_o = 3.83 \times 10^{-4}$ s, $\varepsilon_\infty = 9.15$, $\varepsilon_0 = 32.3$, and again $\rho_0 = 1.22 \times 10^9$ Ω cm.

Parameter estimates obtained from the CUNS-P modulus level fit of figure 9(a) were $\beta_1 = 1/3$ fixed, $\tau_o = 4.37 \times 10^{-5}$ s, $\varepsilon_\infty = 8.84$, $\varepsilon_0 = 33.5$, $\varepsilon_{D\infty} = 6.098$, $\varepsilon_{C1\infty} = 2.738$, and $\rho_0 = 1.22 \times 10^9$ Ω cm. When β_1 was free to vary as well, the CK1S-model results were $\beta_1 = 0.343$, $\tau_o = 5.39 \times 10^{-5}$ s, $\varepsilon_\infty = 8.86$, $\varepsilon_0 = 33.1$, $\varepsilon_{D\infty} = 5.83$, $\varepsilon_{C1\infty} = 3.03$, and $\rho_0 = 1.08 \times 10^9$ Ω cm, and the overall fit was equally good. Fitting at the conductivity level led to a slightly worse fit with $\beta_1 = 0.347$, $\tau_o = 5.84 \times 10^{-5}$ s, $\varepsilon_\infty = 8.92$, $\varepsilon_0 = 32.8$, $\varepsilon_{D\infty} = 5.78$, $\varepsilon_{C1\infty} = 3.13$, and $\rho_0 = 1.09 \times 10^9$ Ω cm. The closely similar parameter
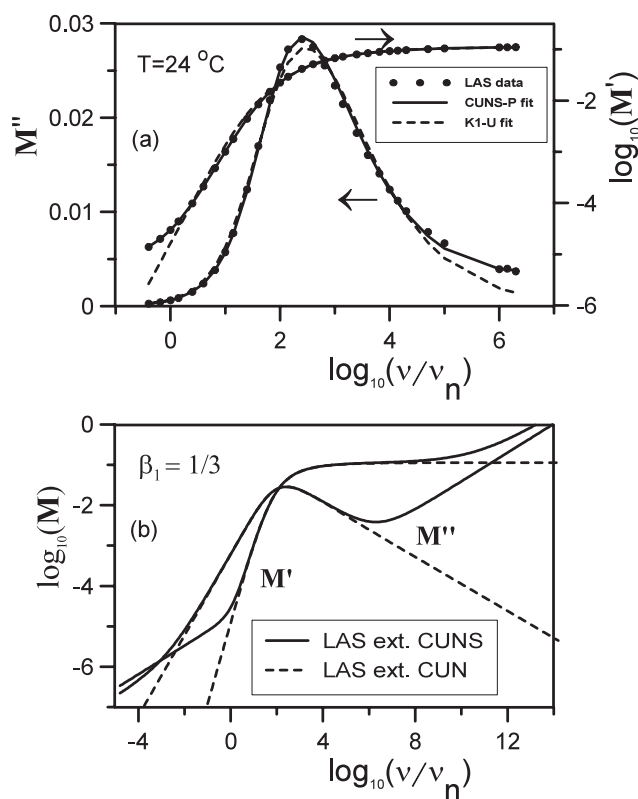
Figure 9. (a) Original $Li_2O \cdot Al_2O_3 \cdot 2SiO_2$ (LAS) data and CK1S complex fit results with $\beta_1 = 1/3$ fixed (the CUNS model) and proportional weighting; and an OMF K1 complex fit with unity weighting and $\beta_1 = \beta_{1M}$ free to vary. (b) Extrapolated responses of the CUNS-model and the CUN-model using the fit parameters obtained from the CUNS fitting of (a), showing both low- and high-frequency effects of electrode polarization, here represented by S, a series constant-phase-element (SCPE) addition to the CUN model.

estimates are a good indication of the consistency of the data and the appropriateness of the fitting model.

Finally, fitting of the imaginary part of the conductivity with $\varepsilon_{D\infty}$ fixed yielded the estimates $\beta_1 = 0.337$, $\tau_o = 4.94 \times 10^{-5}$ s, $\varepsilon_\infty = 8.72$, $\varepsilon_0 = 34.0$, $\varepsilon_{D\infty} = 5.78$ fixed, $\varepsilon_{C1\infty} = 2.94$, and $\rho_0 = 1.09 \times 10^9 \, \Omega$ cm. This fit was not quite as good as that when both real and imaginary parts of the conductivity were simultaneously fitted, but it led to a β_1 estimate even closer to $1/3$. The fit was worse when $\varepsilon_{D\infty}$ was fixed at 0 but led to the estimate $\beta_1 = 0.331$. The reason for holding $\varepsilon_{D\infty}$ fixed when the composite fitting model involves a series electrode-polarization model is discussed in [15]. As discussed in [20], the extreme differences between the OMF M'' estimate of $\beta_1 = 0.468$ and the σ'-fit estimate of 0.33 or 0.34 are a clear indication of the inappropriateness and inconsistency of the OMF approach.

When the OMF β_{1M} estimate of 0.468 is used in the graph of figure 8(b), one obtains an estimate of $\varepsilon_\infty/\varepsilon_{C1\infty}$ of about 3.16, leading, when the estimated value of $\varepsilon_{\infty M} = 9.15$ is used, to the estimate $\varepsilon_{C1\infty} \simeq 2.89$. When the interpolation formula listed in figure 8(b) is used instead, one obtains $\varepsilon_{C1\infty} \simeq 2.59$, a fairly poor estimate of the actual CUNS-model result of 3.13. The resulting $\varepsilon_{D\infty}$ estimate of 6.56 is somewhat larger than the probable value of 6.1.

Finally, the curves in figure 9(b) were calculated from the CUNS-P model parameter estimates for an extended frequency range. They well illustrate the effect of the inclusion of a series electrode polarization part in the full composite fitting model and show that if the data of [7] had involved a wider frequency range, an electrode-polarization explanation of its deviations from the OMF K1-model-fit predictions would doubtless have been proposed much earlier.

Acknowledgment

References

[1] Macdonald J R and Barlow C A Jr 1963 *Rev. Mod. Phys.* **35** 940
[2] Phillips J C 1994 *J. Non-Cryst. Solids* **172–174** 98
[3] Macdonald J R 1987 *J. Appl. Phys.* **63** R51
[4] Macdonald J R 1995 *J. Chem. Phys.* **102** 6241
[5] Macdonald J R 1999 *Braz. J. Phys.* **29** 332
[6] Bőttcher C J F and Bordewijk P 1978 *Theory of Electric Polarization* 2nd edn, vol 2 (New York: Elsevier)
[7] Moynihan C T, Boesch L P and Laberge N L 1973 *Phys. Chem. Glasses* **14** 122
[8] Lindsay C P and Patterson G D 1980 *J. Chem. Phys.* **73** 3348
[9] Macdonald J R 1996 *J. Non-Cryst. Solids* **197** 83
      Macdonald J R 1996 *J. Non-Cryst. Solids* **204** 309 (erratum) In addition, in equation (A2) G_D should be G_{CD}
[10] Macdonald J R 1997 *J. Non-Cryst. Solids* **212** 95 (The symbol σ_0 should be removed from the right end of equation (12))
[11] Macdonald J R 2000 *Inverse Probl.* **16** 1561
[12] Macdonald J R and Brachman M K 1956 *Rev. Mod. Phys.* **28** 393
[13] Macdonald J R and Potter L D Jr 1987 *Solid State Ion.* **23** 61
      Macdonald J R 2000 *J. Comput. Phys.* **157** 280 (The newest WINDOWS version, LEVMW, of the comprehensive LEVM fitting and inversion program, may be downloaded at no cost by accessing http://jrossmacdonald.com It includes an extensive manual and executable and full source code. More information about LEVM is provided at this internet address)
[14] Macdonald J R 2005 *Phys. Rev.* B **71** 184307
[15] Macdonald J R 2005 *J. Phys.: Condens. Matter* **17** 4369
[16] Macdonald J R 1997 *J. Appl. Phys.* **82** 3962
      Macdonald J R 1998 *J. Appl. Phys.* **84** 812
[17] Macdonald J R and Phillips J C 2005 *J. Chem. Phys.* **122** 074510
[18] Macdonald J R 1996 *Electrically Based Microstructural Characterization* (*Symp. Proc.* vol 411) ed R A Gerhardt, S R Taylor and E J Garboczi (Pittsburgh, PA: Materials Research Society) p 71
[19] Macdonald J R 2002 *J. Chem. Phys.* **116** 3401
[20] Macdonald J R 2004 *J. Appl. Phys.* **95** 1849
[21] Macdonald J R 2002 *Solid State Ion.* **150** 263
[22] Scher H and Lax M 1973 *Phys. Rev.* B **7** 4491
[23] Jain H and Krishnaswami S 1998 *Solid State Ion.* **105** 129